Nonlinear, Barotropic Response to a Localized Topographic Forcing: Formation of a "Tropical Surf Zone" and Its Effect on Interhemispheric Propagation

D. W. WAUGH,* L. M. POLVANI,** AND R. A. PLUMB*

*Center for Meteorology and Physical Oceanography, Massachusetts Institute of Technology, Cambridge, Massachusetts
**Department of Applied Physics, Columbia University, New York, New York

(Manuscript received 21 October 1992, in final form 15 July 1993)

ABSTRACT

The nonlinear response of a barotropic, nondivergent, spherical flow representative of the upper troposphere (but without a tropical Hadley cell) to localized, extratropical topographic forcing is examined using high-resolution contour surgery calculations. The response is shown to vary greatly with forcing amplitude and can be significantly different from the linear response. At large amplitude, Rossby wave breaking occurs in the tropics irrespective of the direction of the equatorial winds, and leads to small-scale stirring and the formation of a "tropical surf zone," which inhibits the meridional propagation of the disturbance.

1. Introduction

There have been numerous studies directed toward understanding the influence of orography on stationary planetary waves in the troposphere and on the low-frequency variability of these waves. These studies have shown that the linear response to localized forcing is a downstream wave train (e.g., Hoskins et al. 1977; Grose and Hoskins 1979; Hoskins and Karoly 1981; Webster 1981; Simmons 1982; Webster and Holton 1982; Branstator 1983). The wave train propagates along an arc, which is approximately a great circle, and may cause a significant disturbance a large distance away from the source (including antipodean regions if the winds are westerly at the equator). Therefore, localized forcing, and the corresponding Rossby wave dispersion, has been proposed as a possible mechanism for observed atmospheric teleconnections (e.g., Frederiksen and Webster 1988 and references therein).

For the most part, our conceptual understanding of Rossby wave propagation over the sphere is based on linear calculations or results from models in which nonlinear effects are weak. It is now widely recognized that upper tropospheric waves break in the weak winds at low latitudes, yet the impact of this highly nonlinear process on the larger-scale wave characteristics is poorly understood. This kind of behavior was explicitly modeled by Held and Phillips (1990) in a study of the interaction of a Rossby wave with the Hadley circulation. However, as far as we are aware, there has been no comprehensive, *high-resolution*, study of the *nonlinear* characteristics of planetary wave dispersion on the sphere in a simple setting where the fundamentals of the problem might be better clarified. In this paper we report on a series of high-resolution nonlinear calculations of the response of a barotropic, nondivergent, spherical flow to localized topographic forcing. In particular, we examine the characteristics of wave breaking in the tropics and its effect on the interhemispheric wave propagation. The use of a barotropic model allows an easy understanding of fundamental mechanisms, and also permits a large number of calculations to be performed inexpensively. Previous studies have shown that barotropic models can be very useful in understanding tropospheric stationary waves and atmospheric teleconnections (e.g., Simmons et al. 1983; Lau and Lim 1984; Branstator 1985; Held and Kang 1987; Sardeshmukh and Hoskins 1988).

In order to resolve the details of the wave breaking, we use the method of contour surgery (hereinafter CS; see Dritschel 1988b, 1989), an extension of the contour dynamics method developed by Zabusky et al. (1979). Contour surgery is a numerical method for inviscid flows wherein arbitrarily steep vorticity gradients can be formed, and wherein the scales of motion can vary over a far more extensive range than in conventional pseudospectral modeling. Detailed comparisons between CS and pseudospectral calculations have been made by Legras and Dritschel (1993), and it has been shown that accurate CS calculations can be performed using a moderate number of contours and that the differences between the methods of solution are due to errors in both methods. Waugh (1993) performed further comparisons and showed that realistic CS simu-

Corresponding author address: Dr. Darryn W. Waugh, Dept. of Earth, Atmospheric and Planetary Science, Room 54-1719, MIT, Cambridge, MA 02139.

lations of a topographically forced, barotropic atmosphere can be performed, and that the method is well suited for examining the dynamics of the Rossby wave breaking.

However, the method has some drawbacks that limit the realism with which we can represent the characteristics of atmospheric planetary waves in the tropics. The CS method exploits the exact conservation of potential vorticity and is thus incapable of incorporating nonconservative effects such as those associated with radiation and condensation. Probably the most important consequence of this is our inability to include a Hadley circulation in these calculations.[1] The presence of a Hadley cell is known to have a major influence on the tropical structure of waves propagating from midlatitudes (Farrell and Watterson 1985; Watterson and Schneider 1987; Held and Phillips 1990).

Therefore, results obtained from this model cannot be regarded as representative of the entire tropics. As a boundary condition on our understanding of the whole problem, however, they do show how fully nonlinear Rossby waves would behave in the absence of the Hadley circulation. Moreover, the results should be illustrative of how the waves behave in the upper troposphere tropical "gap" regions where prevailing winds are westerly and the divergent flow is weak. Indeed, it is in these regions of upper tropospheric westerlies that, it has been suggested (Webster and Holton 1982), quasi-stationary Rossby waves may be able to propagate right through the tropics. Indeed, such propagation has apparently been detected (e.g., Thomas and Webster 1994). Linear theory tells us that such propagation cannot occur through easterlies (since the waves would encounter a critical line) nor through very weak westerlies (when their group velocity would be very small). It is of interest (and a major thrust of this paper) to ask how interhemispheric propagation is affected by the occurrence of breaking. For example, consider a linear wave subjected to very weak dissipation propagating through a tropical band of weak westerlies. At sufficiently large amplitude, the wave will break, hence, presumably inhibiting further propagation. We shall in fact show below that this does occur and that propagation is increasingly restricted with larger wave amplitudes.

A second consequence of our assumption of conservative flow is that our results will become unrealistic after long integration. Overturning of the breaking waves in the nonlinear critical layer will quickly, and inevitably, lead to local destruction of the ambient potential gradient and thus create a reflector for the waves (Haynes 1987). One effect of the Hadley cell—and of other nonconservative processes—is to maintain the subtropical gradient and thus to oppose the tendency for the subtropics to become reflective (Held and Phillips 1990). Our calculations, as will be shown below, clearly demonstrate the onset of reflection late in the integrations. Whether this is a realistic representation of real atmospheric behavior is a moot point. For this reason, we do not continue these integrations beyond this stage of dynamical development.

In the next section we outline the model used, the initial zonal flows, the localized forcing, and the method of solution. Results for four calculations with different basic states and forcing amplitude are then given in section 3. These nonlinear calculations show that (for forcing which induces a disturbance of realistic amplitude) there is wave breaking, small-scale stirring in the tropics, and formation of a "tropical surf zone." The nonlinear response is significantly different from that of simple linear models, and the propagation of the disturbance can vary greatly with forcing amplitude. The differences between the wave propagation in these calculations are highlighted in section 4 by examining several diagnostics (perturbation energy density, mean disturbance position, stationary wave activity flux, and surf zone width). The most significant differences between linear and nonlinear calculations occur when there are equatorial westerlies. The effect of the magnitude of these westerlies on the wave propagation is investigated in section 5.

2. Model, initial conditions, and forcing

We consider the response of a inviscid, nondivergent, barotropic spherical model to localized topographic forcing. The materially conserved potential vorticity in this model is

$$Q = \nabla^2\psi + f + F, \tag{1}$$

where ψ is the streamfunction for motion relative to the rotating earth, $f = 2\Omega \sin\varphi$ is the planetary vorticity (Ω being the rotation rate, and φ the latitude), and F is the prescribed quasi-topographic forcing function.

The numerical method of CS is used to perform high-resolution simulations of the response to the localized forcing. Contour surgery has been used by Polvani and Plumb (1992) and Waugh (1993) to perform simulations of a topographically forced polar vortex, and it has been shown that realistic simulations of a topographically forced barotropic atmosphere can be performed. We use the same procedure as in these references, and only a brief description is included here.

In CS calculations the initial Q is piecewise constant. The velocity at a point $\mathbf{x} = (\cos\varphi\cos\lambda, \cos\varphi\sin\lambda, \sin\varphi)$, where (φ, λ) is (latitude, longitude), is then given by

$$\mathbf{u}(\mathbf{x}) = -\frac{1}{2\pi}\sum_{k=1}^{N}\tilde{Q}_k \oint_{C_k} \log(|\mathbf{x} - \mathbf{x}_k|)d\mathbf{x}_k - \mathbf{u}_f(\mathbf{x}) - \mathbf{u}_F(\mathbf{x}), \tag{2}$$

[1] We shall report the results of calculations from a high-resolution pseudospectral model, including a Hadley cell, in a future paper.

where $\mathbf{u}_f = \Omega \cos\varphi \hat{\mathbf{e}}_\lambda$ ($\hat{\mathbf{e}}_\lambda$ is a unit eastward vector) is the velocity due to the planetary vorticity, $\mathbf{u}_F$ is the velocity due to the topographic forcing (see below), N is the number of contours of Q discontinuity, C_k is the boundary of a region of uniform Q, $\tilde{Q}_k$ is the jump in Q across C_k, and $\mathbf{x}_k$ is a point on C_k. The material conservation of Q ensures that Q will remain piecewise constant, and its evolution is then completely determined by the advection of the contours of Q discontinuity.

The contours of Q discontinuity are numerically represented by a series of computational nodes, the velocity at each node is determined from (2), and the evolution of the flow is determined by advecting the nodes by this velocity. To preserve the resolution of the calculations, computational nodes are continually adjusted, with nodes added in regions of high curvature. To enable long time calculations, contours are disconnected and reconnected so as to remove filamentary structures smaller than some prescribed cutoff scale [full details of the contour representation and the surgery procedure are given in Dritschel (1988b, 1989)].

In all calculations performed, the initial basic state is zonally symmetric with zonal velocity

$$u(\varphi) = \alpha_1 \cos\varphi + \alpha_2 \sin 2\varphi + \alpha_3 \sin^2 2\varphi, \quad (3)$$

where the constants α_i are chosen so that the winds are representative of the upper troposphere during the Northern Hemisphere winter. Three basic states with the same jet structure but different equatorial winds are shown in Fig. 1: basic state $\mathscr{E}_1$ has weak equatorial easterlies, basic state $\mathscr{W}_1$ has weak equatorial westerlies, and basic state $\mathscr{W}_2$ has strong equatorial westerlies. To perform CS calculations, the continuous Q profiles are discretized into a finite number of regions of uniform Q. The initial position and discontinuity in Q across each contour are determined so as to minimize, in a least-squares sense, the difference between the continuous and discrete Q profiles.

The topographic forcing in the calculations corresponds to a circular region (with solid angle θ_0) of uniform vorticity $F_0\Omega T(t)$ (where $T(t) = 1 - e^{-t/\tau}$ is a time-dependent factor that introduces the forcing smoothly) centered at (longitude, latitude) = (λ_0, φ_0). The velocity corresponding to this forcing is

$$\mathbf{u}_F(\mathbf{x}, t) = -0.5 F_0 \Omega T(t) \times (1 \pm \cos\theta_0)(\mathbf{x} \wedge \mathbf{x}_0)/(1 \pm \mathbf{x}\cdot\mathbf{x}_0), \quad (4)$$

where $\mathbf{x}_0$ is the center of the forcing, and the plus (minus) sign corresponds to the velocity inside (outside) the circular forcing region.

In all calculations presented in this paper $N = 21$ contours are used to represent the initial state (calculations using larger N were performed and the results were found to be independent on N). The time step used is $1/20$ of a day, and the surgery scale below which filamentary features are removed is $\delta \approx 18$ km.

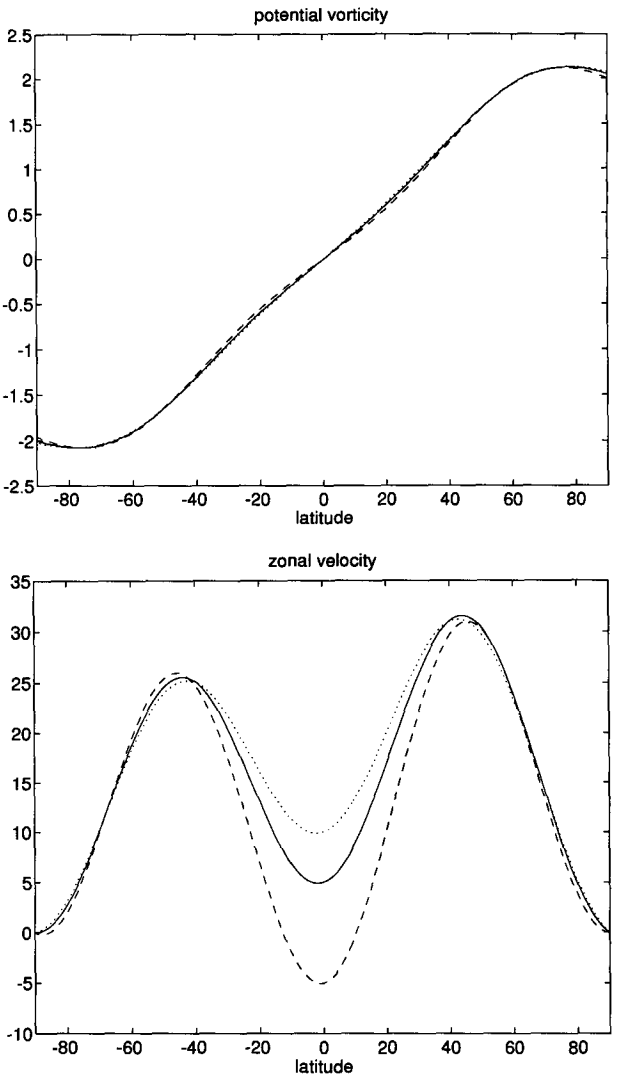

FIG. 1. Profiles of initial (a) potential vorticity Q_0, in units of rotation rate Ω, and (b) zonal velocity u_0, in m s^{-1}, for basic states $\mathscr{E}_1$ (dashed curve), $\mathscr{W}_1$ (solid curve), and $\mathscr{W}_2$ (dotted curve). The zonal velocity is given by (3) with $(\alpha_1, \alpha_2, \alpha_3)$ equal to $(-5, 2.5, 32)$ for $\mathscr{E}_1$, (5, 3, 25) for $\mathscr{W}_1$, and (10, 3, 21) for $\mathscr{W}_2$.

3. Results

We have carried out an extensive series of computations varying the amplitude, position, and form of the forcing, and the initial basic state. In this section we discuss the results from four representative calculations in which only the forcing amplitude and initial basic state are varied. The four calculations are a small amplitude forcing case and a large amplitude forcing case for the basic states $\mathscr{E}_1$ and $\mathscr{W}_1$; see Table 1. Calculations with other forcing amplitudes and with basic state $\mathscr{W}_2$ are discussed in sections 4 and 5.

In the following subsections, the response to the localized forcing in these calculations is examined by

TABLE 1. Parameters for calculations shown in this paper. In all calculations the forcing corresponds to a circular region (with solid angle $\theta_0 = 10°$) of vorticity centered at $(\lambda_0, \varphi_0) = (90°, 40°)$. The forcing is turned on slowly with $\tau = 2$ days. The basic states $\mathcal{W}_1$ and $\mathcal{E}_1$ are shown in Fig. 1.

Calculation	Basic state	Amplitude F_0
W05	$\mathcal{W}_1$	0.05
E05	$\mathcal{E}_1$	0.05
W20	$\mathcal{W}_1$	0.20
E20	$\mathcal{E}_1$	0.20

plotting the Q contours from the CS calculations, and also the perturbation streamfunction $\psi^* = \psi - \psi_0$ (ψ_0 is the initial zonally symmetric streamfunction). Here ψ is calculated from the Q contours using the contour integral expression given in Polvani and Dritschel (1993). Figure 2 shows the initial position of the Q contours (for basic state $\mathcal{W}_1$) and the circular forcing region. The evolution of Q shows the formation of Rossby waves, their breaking, and the generation of small-scale structures, while the evolution of ψ^* highlights the propagation of the disturbance. In section 4 the propagation of the disturbance is quantified using several diagnostics.

a. Small amplitude forcing

We first consider the case of small amplitude forcing, and compare the results with previous linear calculations (e.g., Hoskins et al. 1977; Grose and Hoskins 1979; Hoskins and Karoly 1981).

Figures 3 show the evolution of Q and ψ^* for weak forcing in the basic state with tropical westerlies (calculation W05). These plots show the development of a wave system east of the forcing region (marked by a cross). The Rossby waves do not break (i.e., no irreversible deformations occur) and the response is as in previous linear calculations: an eastward traveling Rossby wave train is formed that has a double structure (this can be seen more clearly in the wave activity flux vectors; see section 4), a strong NE–SW tilt in the Northern Hemisphere, and propagates equatorward [the two components travel approximately along great circles as predicted by linear theory, e.g., Longuet-Higgins (1964); Hoskins et al. (1977)]. The disturbance crosses the equator into the antipodean region and then around the sphere to the source region [it takes around 20 days for the disturbance to propagate around the sphere, consistent with the results of Hoskins et al. (1977)]. Previous studies have included dissipation and the waves have very small amplitude by the time they have gone around the sphere (and hence, there is very little interference with the source region). The quasi-steady state reached in this calculation (with no dissipation) is therefore different from that reached in previous calculations.

The response when the basic state has tropical easterlies (calculation E05) is very different from the above calculation. The initial response to the forcing is again a wave system downstream of the source, but now the Rossby waves break near the zero wind line—to the north of the equator (see Fig. 4a). This breaking first occurs slightly east of the forcing and then propagates around the sphere to form a confined region of breaking. The deformation of the Q contours and subsequent wave breaking is in qualitative agreement with nonlinear Rossby wave critical layer theory (e.g., Haynes 1987 and references therein), and the breaking zone is centered around the critical line (see Fig. 12b below). Note that the wave breaking in Fig. 4a would not be observed in low-resolution calculations with dissipation and diffusion. The equatorward propagation of the disturbance in this calculation is inhibited by breaking zone and there is very little cross-equatorial prop-

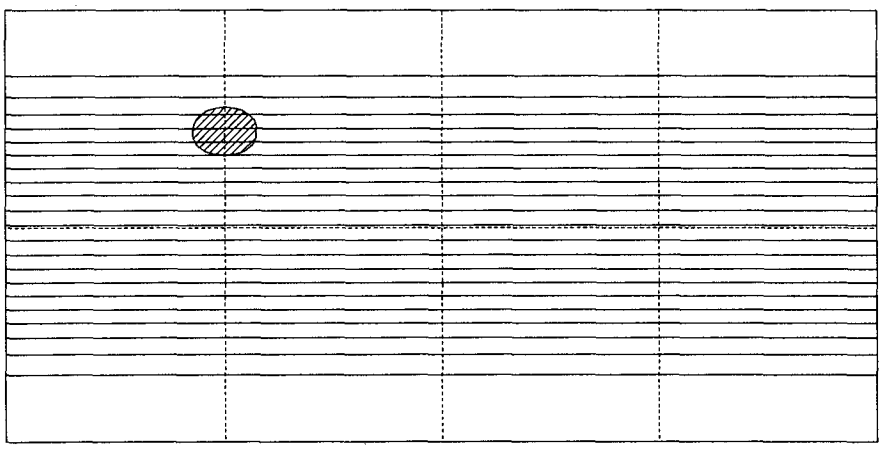

FIG. 2. Latitude–longitude plot of initial Q contours in the CS calculations for basic state $\mathcal{W}_1$ (the position of the contours is very similar for the basic states $\mathcal{W}_2$ and $\mathcal{E}_1$). The shaded region corresponds to the topographic forcing region.

agation; see Fig. 4b. The wave breaking absorbs most of the disturbance, although there is some suggestion of reflection back to higher latitudes, and only small transients propagate into the Southern Hemisphere. Previous studies have shown that equatorial easterlies inhibit cross-equatorial propagation (e.g., Hoskins et al. 1977; Grose and Hoskins 1979; Hoskins and Karoly 1981; Webster and Holton 1982), but they have included numerical dissipation in their calculations so that waves are absorbed at the critical line and there is no reflection. The characteristics of the breaking zone are discussed further in the next subsection.

b. *Large amplitude forcing*

We now consider the response to larger amplitude forcing. Figure 5 shows the evolution of Q and ψ^* for the calculations with the basic state with equatorial westerlies and $F_0 = 0.2$ (calculation W20). Although the initial response is similar to the small amplitude case (cf. day 7 in Figs. 3b and 5b), the subsequent response is very different. There is now Rossby wave breaking and the response is nonlinear. As in calculation E05, the breaking first occurs southeast of the forcing region and then propagates around the sphere and forms a breaking zone south of the forcing. As with stratospheric planetary wave breaking forming the well-known "surf zone" surrounding the polar vortex (McIntyre and Palmer 1983, 1984), the wave breaking here forms a "tropical surf zone" (Held and Phillips 1990). The breaking in calculation W20 is more vigorous than the small forcing case, and there is a large amount of stirring with small-scale filamentary and coherent features generated. Note that the finescale features in the surf zone are not seen in the streamfunction field (cf. Figs. 5a and 5c). Previous studies have generally focused on the streamfunction or geopotential height fields, and have therefore not been able to reveal small-scale filaments and mixing. Calculations with different forcing amplitudes show that the amount of breaking and the extent of the surf zone increases with amplitude (see section 4d). One of the main consequences of the wave breaking is the weaker response in the Southern Hemisphere (relative to that in the Northern Hemisphere), as can be seen in Fig. 5b. Whereas in the small amplitude (linear) case the disturbance propagates across the equator (Fig. 3b), most of the disturbance is now absorbed or reflected by the surf zone. Therefore, although linear calculations suggest that there may be significant propagation through equatorial westerlies this may not be the case when nonlinear effects become important.

For sufficiently large amplitude forcing to the basic state with tropical easterlies (calculation E20), the response is qualitatively the same as for the westerly case; see Fig. 6. A tropical surf zone is formed that absorbs or reflects most of the disturbance, and there is only a small response south of this zone. The breaking zone in calculation E20 occurs north of that in W20, and the cross-equatorial response in E20 is smaller. Comparing the small and large amplitude forcing experiments for the basic state $\mathscr{E}_1$ we see that, although the response in both cases is Rossby wave breaking and the formation of a critical layer, the disturbance propagation is different for the two experiments (cf. Figs. 4b and 6b) and the response is indeed nonlinear.

The above calculations suggest that for large amplitude forcing, the response is not as sensitive to the direction of the equatorial winds as in small amplitude (linear) calculations. For large forcing, breaking occurs in the tropics (whether or not there is an initial critical line) and the cross-equatorial response is small; this is quantified in the next section.

4. Diagnostics

In this section we use various diagnostics to quantify the propagation of the disturbance in the above calculations, and also to highlight the differences between the calculations.

a. *Perturbation energy*

The differences in the meridional propagation in the above calculations can be clearly seen by considering the latitudinal structure of the perturbation energy density $E^* = \frac{1}{2}(u^{*2} + v^{*2})$ (where (u^*, v^*) is the perturbation velocity. Figure 7 shows that the latitudinal variation of the zonal average of the energy density $[E^*]$ at day 35 for the four calculations shown in the previous section ($[E^*]$ for the small amplitude forcing cases has been scaled by the square of the ratio of the forcing amplitudes, that is, $(0.20/0.05)^2 = 16$). Only in the small amplitude case with equatorial westerlies is there substantial cross-equatorial propagation. In the other cases, the wave breaking (and formation of a surf zone) inhibits the interhemispheric propagation of energy, and there is a buildup of energy in the Northern Hemisphere. The buildup of energy in the surf zone is presumably due to accumulation of wave activity, whereas the buildup at higher latitudes is suggestive of reflection from the breaking region. Note that the latitudinal variation of the energy density at other times shows the same qualitative behavior, although there is an increase in magnitude with time and some variation in the fluctuations in the curves.

The effect of the wave breaking on interhemispheric propagation can be seen in Fig. 8, which shows the Northern and Southern Hemisphere perturbation energy density for a series of calculations with varying forcing amplitude F_0. As F_0 is increased, the amount of wave breaking increases (see section 4d) and the relative amount of energy in the Southern Hemisphere decreases. Comparing results for the nonlinear calculations for the basic state $\mathscr{W}_1$ with that predicted by linear theory (the solid curves in Fig. 8 correspond to

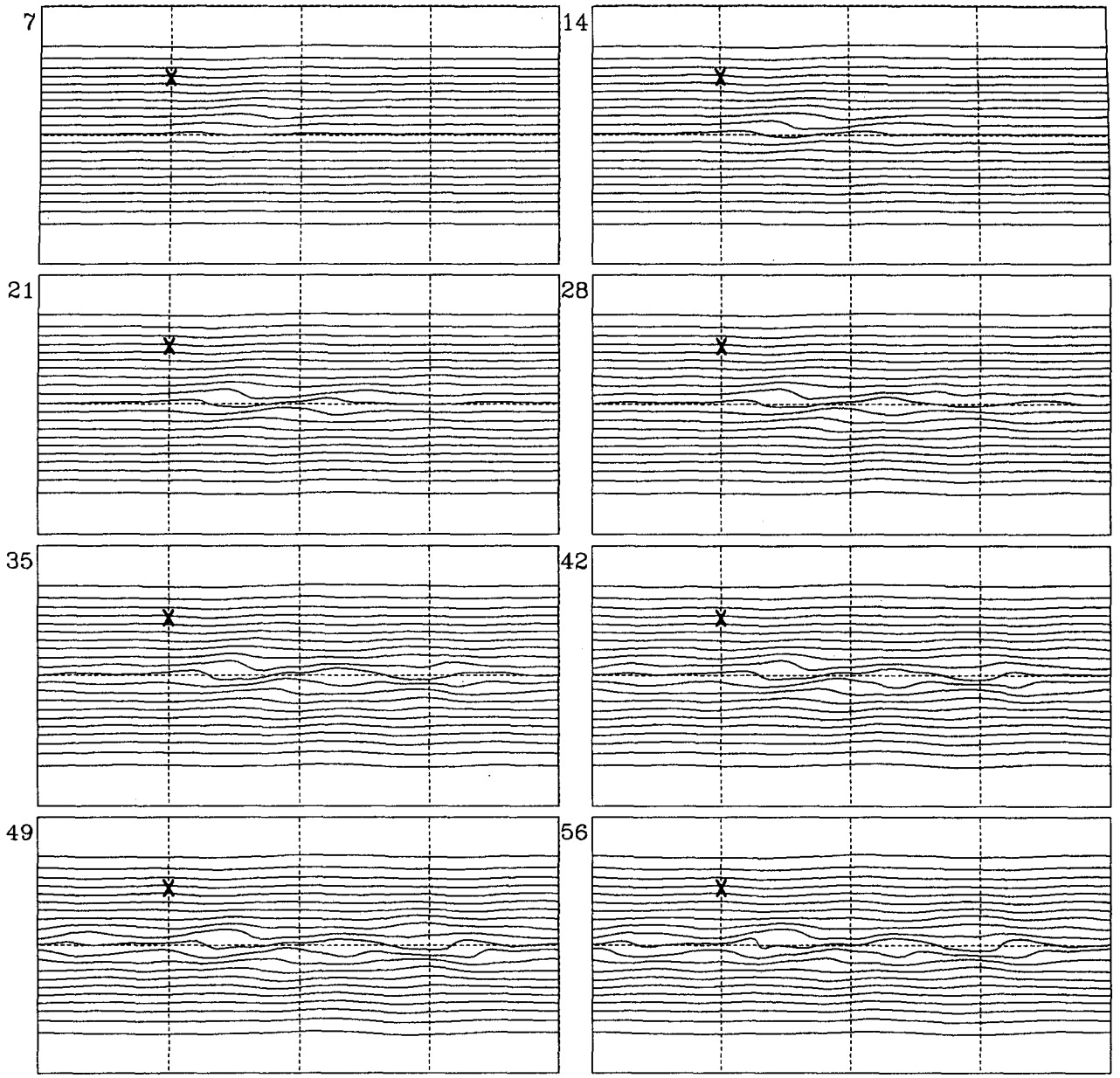

FIG. 3. Evolution of (a) potential vorticity Q, and (b) perturbation streamfunction ψ^* for forcing amplitude $F_0 = 0.05$ and basic state W (calculation W05). Plots are on global latitude–longitude grid, and the center of the forcing is marked by the cross. Time is in days and is

the energy density predicted by inviscid linear theory using the values from a CS calculation with $F_0 = 0.025$), we see that linear calculations overpredict the propagation into the Southern Hemisphere and underpredict the response in the Northern Hemisphere.

b. *Angular pseudomomentum*

Another method to quantify the meridional propagation of the disturbance is to use the angular pseudomomentum to define a mean disturbance position (Waugh 1993). Combining the invariants of area within each contour and angular impulse, it is possible to form the quantity (Dritschel 1988a)

$$P = \sum_k^N P_k = -\frac{1}{2}\sum_k^N \tilde{Q}_k \oint_{C_k} \eta_k^2(\lambda, t)d\lambda, \quad (5)$$

which is exactly quadratic in the disturbance amplitude ($\eta_k = z_k - z_{k0}$ being the displacement from the basic

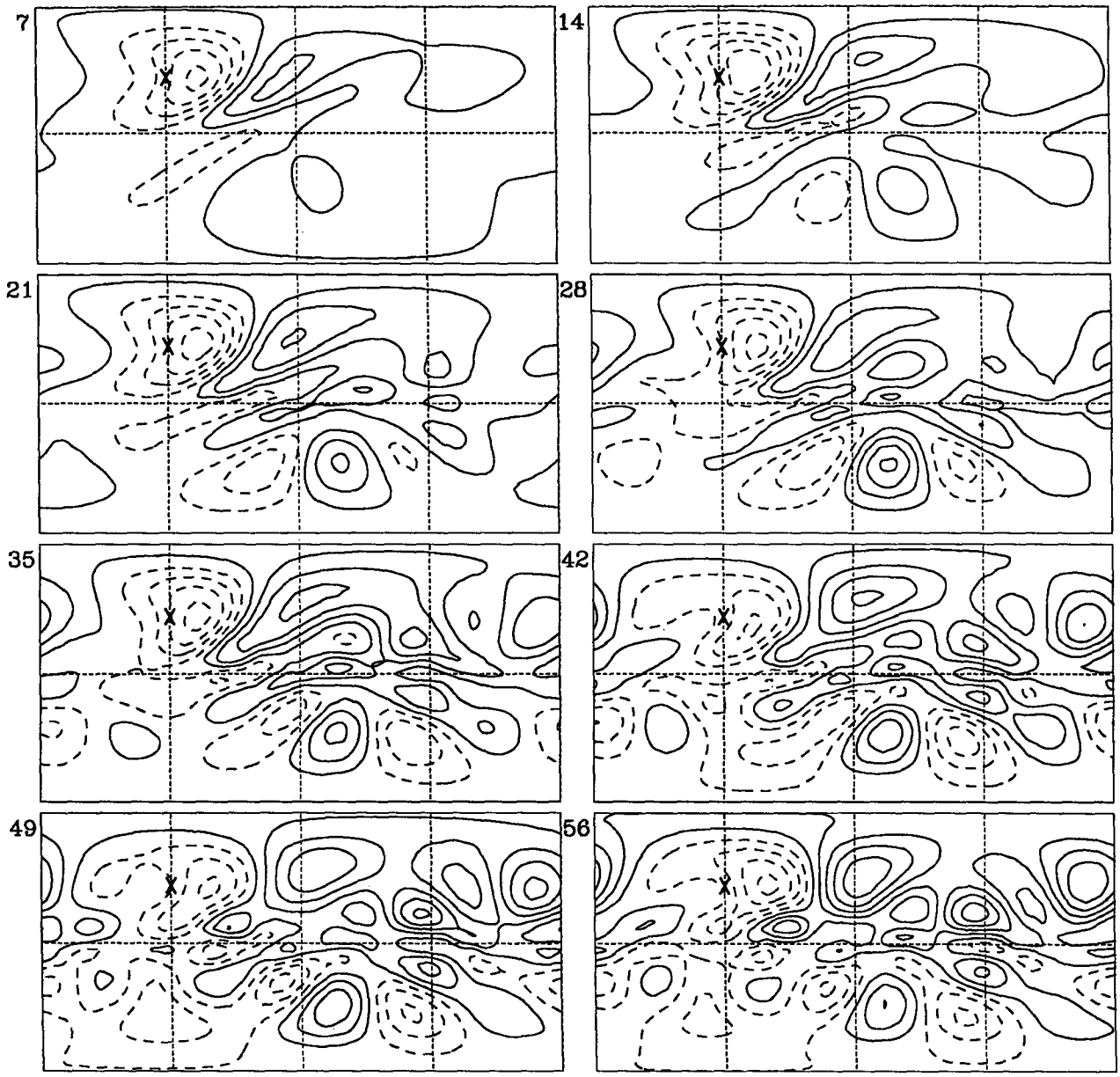

FIG. 3. (*Continued*) to the upper left of each plot. The contour interval for the ψ^* plots is 1.25×10^6 m^2 s^{-1}.

state z_{k0} and $z = \sin\varphi$). Here P is the angular pseudomomentum (McIntyre and Shepherd 1987) for piecewise constant Q distributions, and is of definite sign if all $\tilde{Q}_k$ have the same sign and as such bounds the disturbance growth (and decay) in the absence of forcing.

The normalized contribution of each contour to the angular pseudomomentum, $\hat{P}_k = P_k/P$, gives a measure of how each contour retains its initial wave activity. Furthermore, it can be used to define a mean disturbance position

$$\bar{z} \equiv \sum_k^N \hat{P}_k z_{k0}. \qquad (6)$$

Figure 9 shows the variation of $\bar{\varphi} = \sin^{-1}(\bar{z})$ with time for the four representative calculations. Again we see that the southward propagation is larger when there is weaker forcing and when there are equatorial westerlies. When there is no Rossby wave breaking (calculation W05), the mean disturbance position propagates near to the equator, but when breaking occurs the disturbance propagates only as far as the surf zone.

c. *Wave activity flux*

To investigate the two-dimensional propagation of the disturbance we use the stationary wave activity flux:

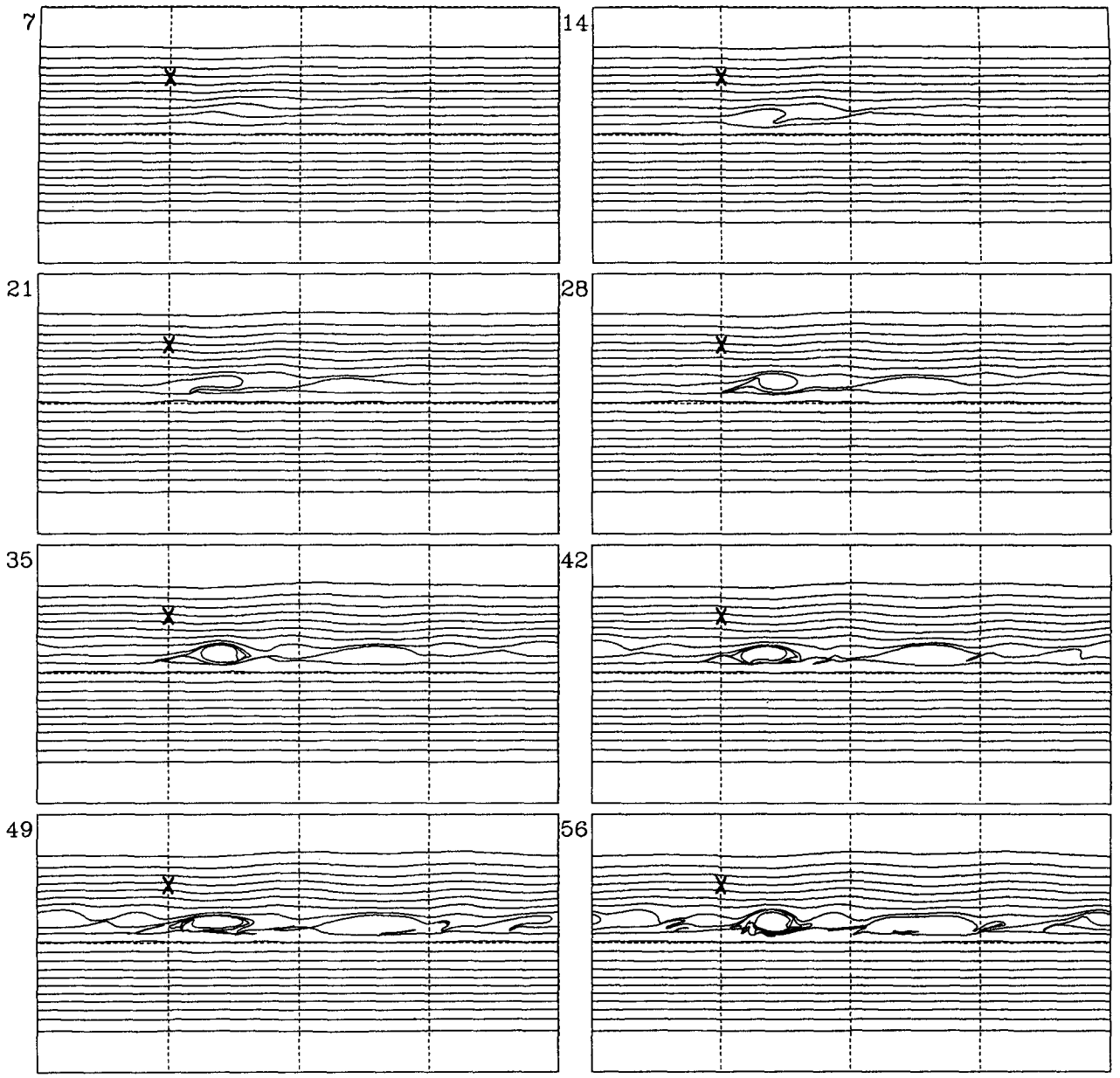

FIG. 4. As in Fig. 3 except initial condition is basic state $\mathscr{E}_1$ (calculation E05).

$$\mathbf{F} = \frac{1}{2a^2 \cos\varphi}\left(\left(\frac{\partial\psi^*}{\partial\lambda}\right)^2 - \psi^*\frac{\partial^2\psi^*}{\partial\lambda^2}, \quad \frac{\partial\psi^*}{\partial\lambda}\frac{\partial\psi^*}{\partial\varphi} - \psi^*\frac{\partial^2\psi^*}{\partial\lambda\partial\varphi}\right) \quad (7)$$

Plumb (1985). Here $\mathbf{F}$ is the two-dimensional extension of the Eliassen–Palm flux (the zonal average of $\mathbf{F}$ is equal to the EP flux apart from an unimportant zonal component) and has all the same properties as an indicator of wave propagation.

Figure 10 shows the wave activity flux $\mathbf{F}$, and also the perturbation streamfunction ψ^*, at day 7 for calculation W05. The plots for all four calculations are similar at day 7, and have the same characteristics as the flux for the linear calculation in Plumb (1985). The pattern of $\mathbf{F}$ is consistent with the earlier interpretation of ψ^*, that is, the formation of a wave train eastward of the source. The strongest divergence of $\mathbf{F}$, and therefore export of wave activity, occurs southeast of the source.

As has already been noted, although the initial response is similar in all calculations, there are large dif-

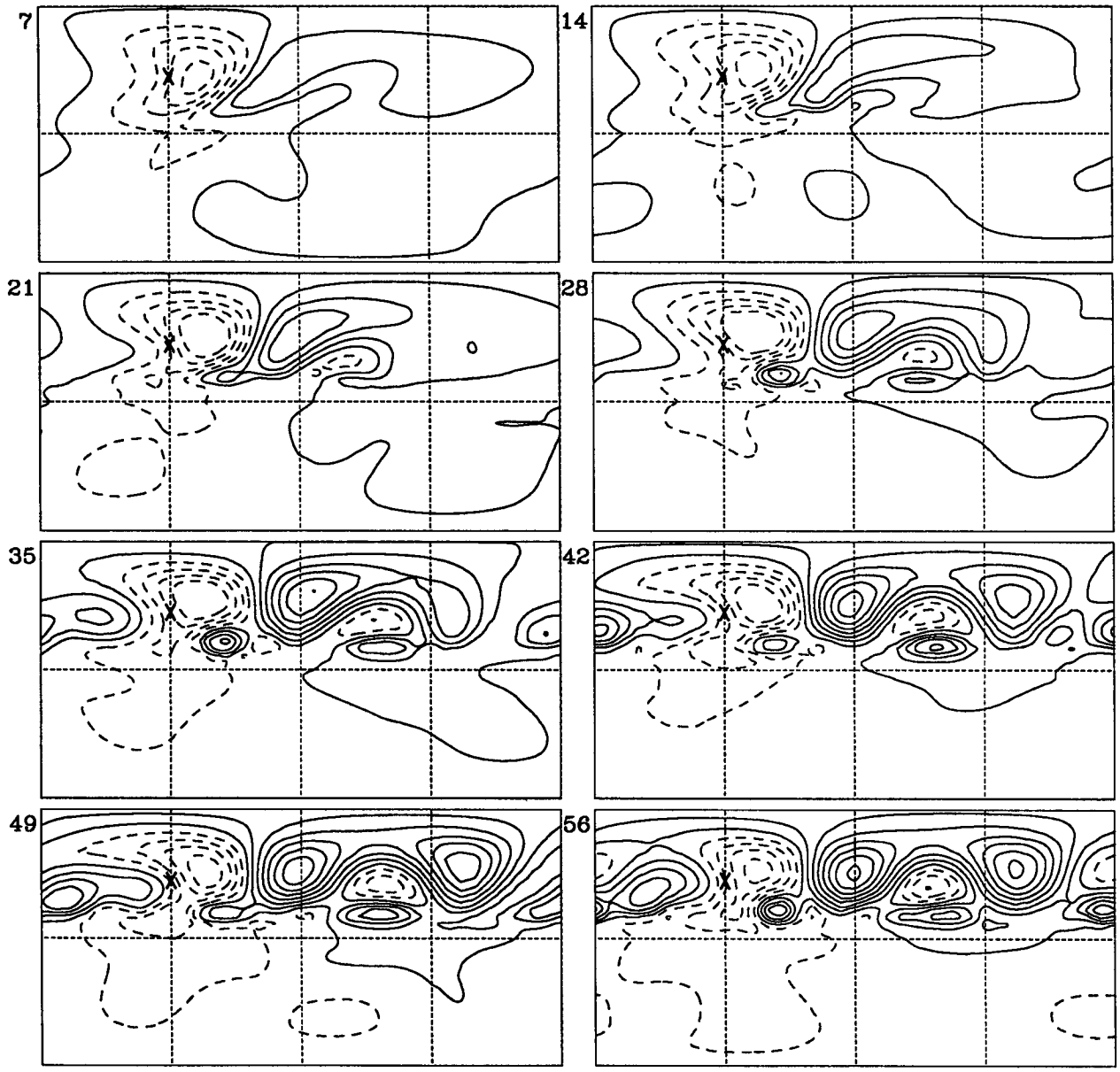

FIG. 4. (*Continued*)

ferences at later times. The differences can be clearly seen from the wave activity flux. Figure 11 shows **F** at day 35 for all four calculations. The plot for calculation W05 clearly shows the propagation of wave activity around the globe. It also shows the wave train splitting into a double structure; a SE component and a NE component. The NE traveling wave turns equatorward before it reaches the North Pole [consistent with linear theory of Hoskins et al. (1977)]. The plots for the other three calculations are very different from this calculation. Although the wave train still has a double structure, there is now very little propagation of wave activity into the Southern Hemisphere. The wave activity is absorbed and partly reflected by the breaking zone [there are suggestions of reflection from the tropical breaking zone, e.g., near 20°N, 45°W in Figs. 11b, 11c, and 11d. The two plots for $F_0 = 0.20$ are qualitatively similar although there is propagation farther south when there are westerlies in the tropics (as shown earlier).

d. Surf zone width

To see how the width of the region of Rossby wave breaking varies with forcing amplitude and basic state,

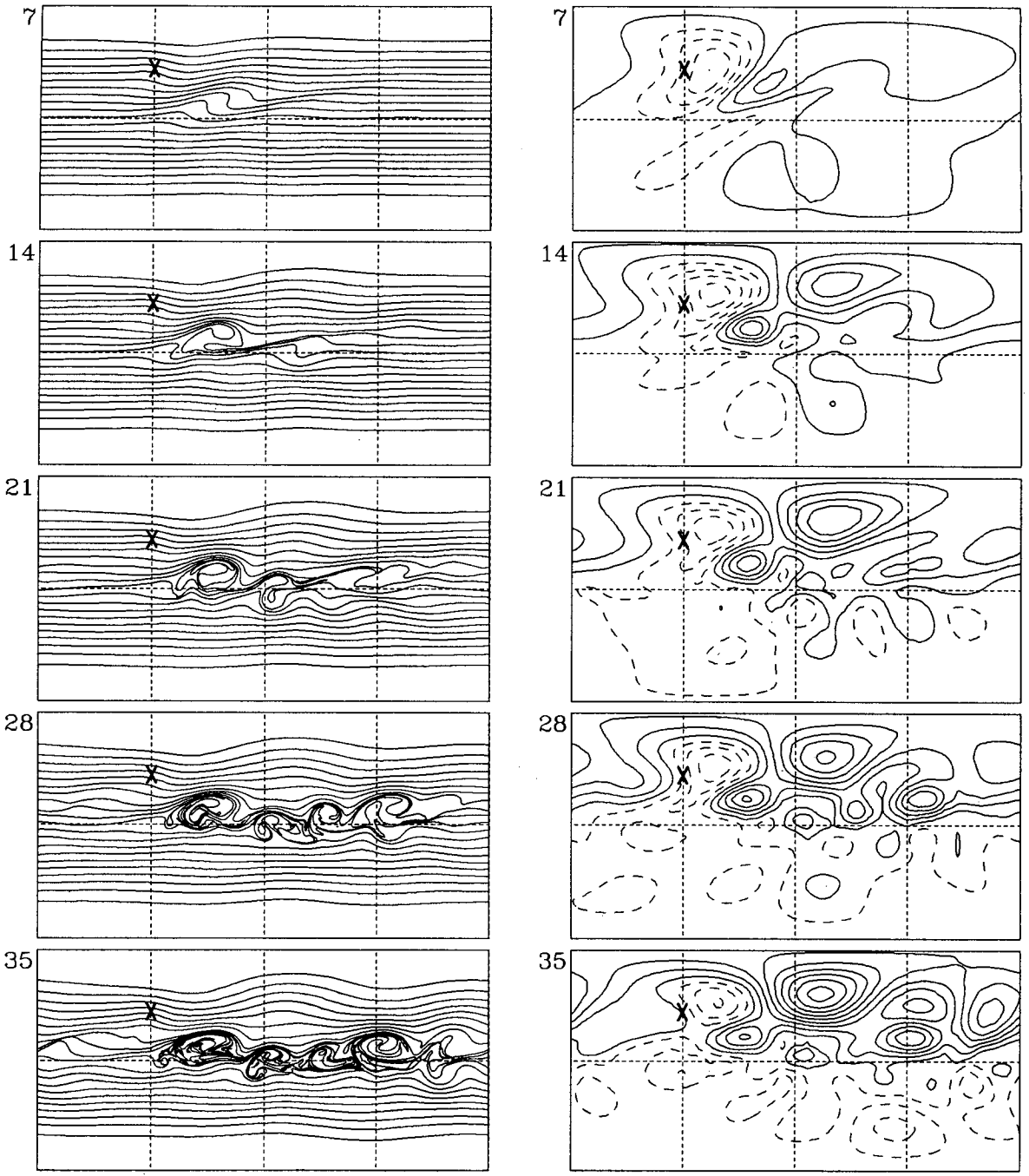

FIG. 5. (a) and (b) As in Fig. 3 except $F_0 = 0.20$ (calculation W20) and ψ^* contour interval is 5×10^6 m^2 s^{-1}.

we have performed a series of calculations with varying amplitude and basic state. We define the surf zone by the region where there is overturning in the PV contours, that is, double-valued contours signify the onset of irreversible deformation and breaking. From the CS calculations we can then determine the boundary of the surf zone to within the spacing of the initial contours. For example, in calculation W20 the seven most northern contours are single valued at day 35 but the eighth contour is double valued (see Fig. 5a), and so the northern boundary of the surf zone is between $\varphi = 24.586°$ and $\varphi = 19.967°$ (the initial position of the seventh- and eighthmost northern contours).

Figures 12a and 12b show the variation in the surf zone width with F_0 for calculations with basic state $\mathscr{W}_1$ and $\mathscr{E}_1$, respectively. In both cases the width of the surf

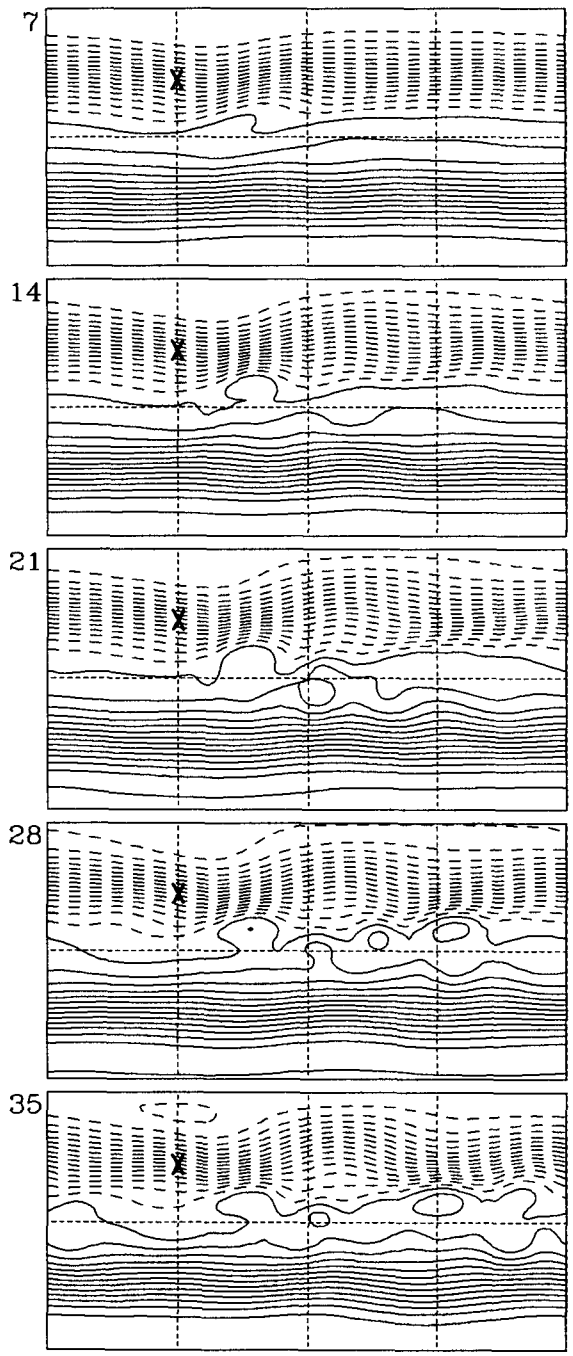

FIG. 5. (*Continued*) (c) Evolution of the streamfunction ψ (contour interval is 1×10^7 m^2 s^{-1}).

zone increases with forcing amplitude. The upper boundary increases approximately linearly whereas, for large forcing, the lower boundary is approximately constant. For calculations with basic state $\mathscr{E}_1$ wave breaking occurs for all amplitudes, and the breaking zone is centered around the critical line ($\varphi_{crit} = 10.4°$). For the basic state $\mathscr{W}_1$ there is a critical amplitude for onset of breaking (which is in the range $0.06 < F_0 < 0.0625$), and the surf zone is centered around the equator (where the initial westerlies are weakest).

As discussed in Polvani et al. (1989) and Polvani and Plumb (1992), the onset of breaking is associated with the existence of a stagnation point in the flow. Breaking occurs when a stagnation point is coincident with a contour. For the basic state $\mathscr{E}_1$ there is initially a critical line and breaking occurs for all forcing amplitudes, whereas for the basic state $\mathscr{W}_1$ there is a critical amplitude for the development of stagnation points (and hence breaking). Using the results from a calculation with $F_0 = 0.025$ (in which there is no breaking), linear theory predicts that stagnation points develop for $F_0 \geq 0.0625$. This implies that wave breaking will occur when $F_0 \geq 0.0625$, consistent with the results from the nonlinear calculations (see Fig. 12a). Thus, linear theory appears to give good guidance for prediction of when breaking will occur.

5. Magnitude of the equatorial westerlies

It has been shown that even if there is no critical line (i.e., equatorial westerlies), wave breaking occurs if the forcing is above a critical amplitude. We now investigate the dependence of this critical amplitude, and also that of the interhemispheric propagation, on the magnitude of the basic-state tropical westerlies by considering the evolution for basic state $\mathscr{W}_2$. This basic state has the same jet structure as $\mathscr{W}_1$ (and also $\mathscr{E}_1$) but has stronger equatorial westerlies (10 m s^{-1} compared with 5 m s^{-1}); see Fig. 1.

The results for this basic state $\mathscr{W}_2$ are qualitatively the same for $\mathscr{W}_1$. For small amplitude forcing there is no wave breaking, whereas for forcing above a critical amplitude breaking occurs and a surf zone is formed. The amount of breaking and the width of the surf zone increase with forcing amplitude, and the wave breaking inhibits the interhemispheric propagation.

There is, however, significant variation in the quantitative results. The critical amplitude for amplitude for breaking is larger for basic state $\mathscr{W}_2$ ($F_0 \approx 0.085$ compared with $F_0 \approx 0.0625$). The critical value is again consistent with the formation of stagnation points as predicted by a small amplitude calculation together with linear theory. For the same forcing amplitude there is less breaking and greater cross-equatorial propagation with the basic state $\mathscr{W}_2$ than with $\mathscr{W}_1$. Figure 13 shows the Southern Hemisphere energy density for the two westerly basic states from nonlinear calculations ($\mathscr{W}_1$: crosses, $\mathscr{W}_2$: circles) and from linear theory ($\mathscr{W}_1$: dashed curve, $\mathscr{W}_2$: solid curve). In both cases linear theory overpredicts the cross-equatorial response, but larger forcing (and breaking) is required when there are stronger westerlies for the difference to be significant. Note that the amount of breaking and the width of surf zone for $F_0 = 0.3$ with basic state $\mathscr{W}_2$ is comparable with that for $F_0 = 0.2$ with $\mathscr{W}_1$.

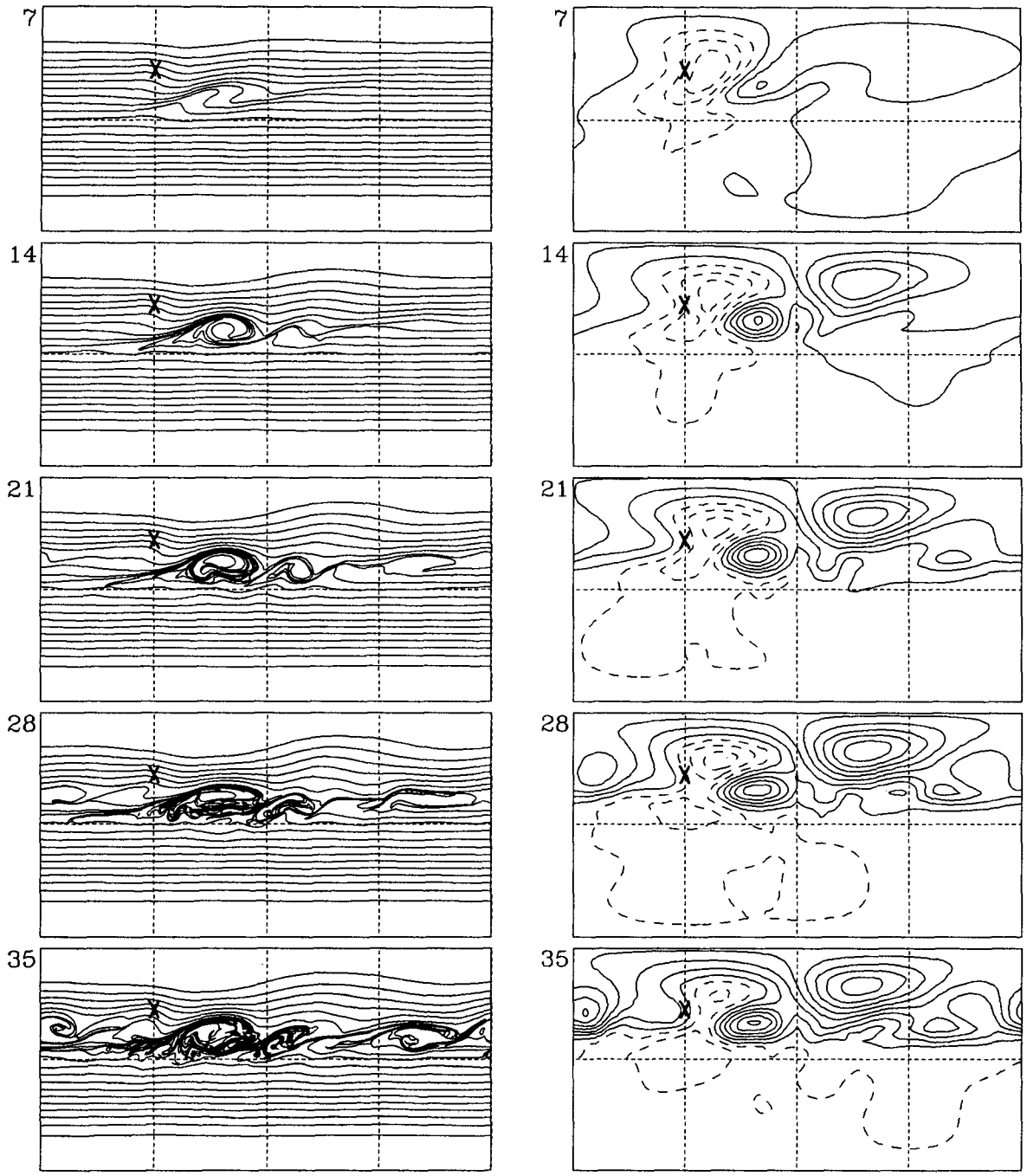

FIG. 6. As in Fig. 5 except initial condition is basic state $\mathscr{E}_1$ (calculation E20).

6. Discussion

The calculations in this paper show that in an inviscid, nondivergent, barotropic atmosphere there is a significant variation in interhemispheric wave propagation with the amplitude of the localized forcing. The nonlinear response for large amplitude forcing is significantly different from that predicted by linear models.

The results from small amplitude experiments are consistent with previous linear calculations. The response to weak forcing is composed of Rossby wave trains that propagate eastward (and approximately

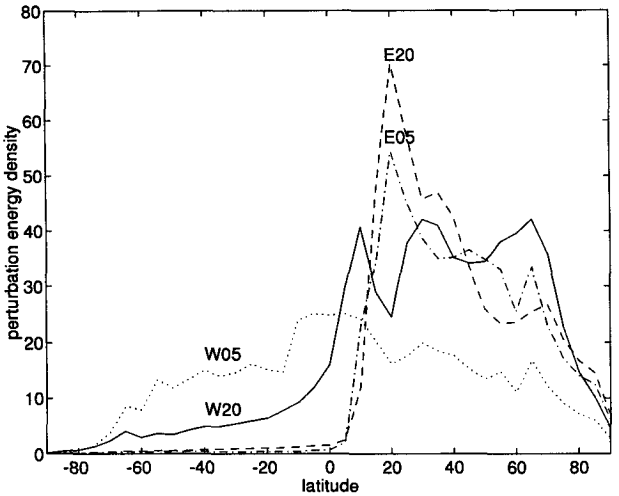

FIG. 7. Latitudinal structure of the zonal average of the perturbation energy density $[E^*]$ (in $m^2\ s^{-2}$) at day 35 for calculations W05 (dotted curve), E05 (dot–dashed curve), W20 (solid curve), and E20 (dashed curve). Here, $[E^*]$ has been scaled by the square of the ratio of the forcing amplitudes, i.e., $(0.20/0.05)^2 = 16$, in the small amplitude forcing cases (W05 and E05).

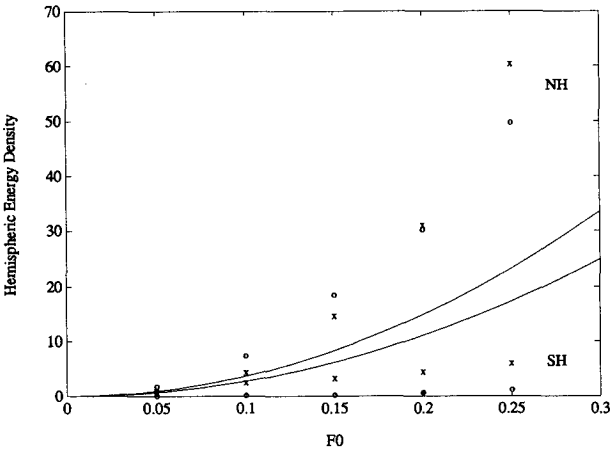

FIG. 8. Hemispheric perturbation energy ($m^2\ s^{-2}$), at day 35, for a series of calculations with various F_0. A cross corresponds to a calculation with basic state $\mathcal{W}_1$, and a circle to calculations with basic state $\mathcal{E}_1$. In both cases the higher value for given F_0 corresponds to the Northern Hemisphere and the lower to the Southern Hemisphere. The solid curves correspond to the energy density in the Northern (upper curve) and Southern (lower curve) Hemisphere for basic state $\mathcal{W}_1$ predicted by linear theory using the values from a calculation with $F_0 = 0.025$.

along great circles). If there are equatorial westerlies the disturbance propagates into the other hemisphere (and around the globe), whereas there is only a small response in the antipodean region if there are equatorial easterlies (and hence a critical line).

In the nonlinear regime, the occurrence of Rossby wave breaking leads to the formation of a tropical surf zone (the extent of which varies with the forcing amplitude). Within this surf zone finescale structures are generated and small-scale stirring occurs (with material being mixed across the extent of the surf zone). The Rossby wave breaking occurring in the tropical surf zone inhibits the meridional propagation of the disturbance and the cross-equatorial response is smaller than that predicted by linear theory. The amplitude of the forcing for the onset of breaking (and for nonlinearities to become important) increases with the magnitude of the equatorial westerlies.

To estimate which flow regime (i.e., forcing amplitude) in this simple barotropic atmosphere is most relevant to the real atmosphere, we compare the magnitude of the response in the above calculations with that observed in the upper troposphere. The observed maximum $[E^*]$ in the upper troposphere for December to February analyses is in the range 60 to 100 $m^2\ s^{-2}$ (e.g., Lau et al. 1981; Lau 1984). Comparison with Fig. 8 indicates that the amplitude $F_0 = 0.2$ is much closer to the observations than $F_0 = 0.05$. Therefore, of the calculations reported here, those with large amplitude forcing (and therefore significant wave breaking even in the case of strong tropical westerlies) will give the best insight into the response of the atmosphere to localized forcing. It therefore seems important to consider the effect of wave breaking in theories of interhemispheric propagation.

In the CS calculations presented the flow is nondivergent and the only dissipative effect is that due to the removal of some small-scale features (by surgery). We have compared these calculations with a similar series of experiments using a high-resolution (T85) pseudospectral code to solve the spherical shallow-water equations. There is very good agreement between the two series of experiments: at sufficiently high resolution the shallow-

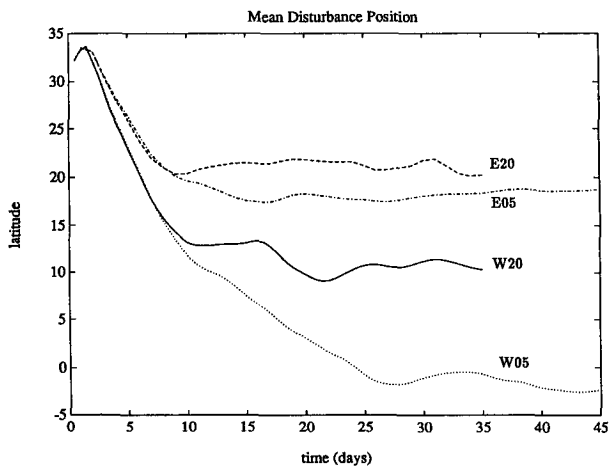

FIG. 9. Temporal variation of mean disturbance position $\bar{\varphi}$, see (6), for the four calculations shown in Figs. 2 to 6. The curve types for each calculation are the same as in Fig. 7.

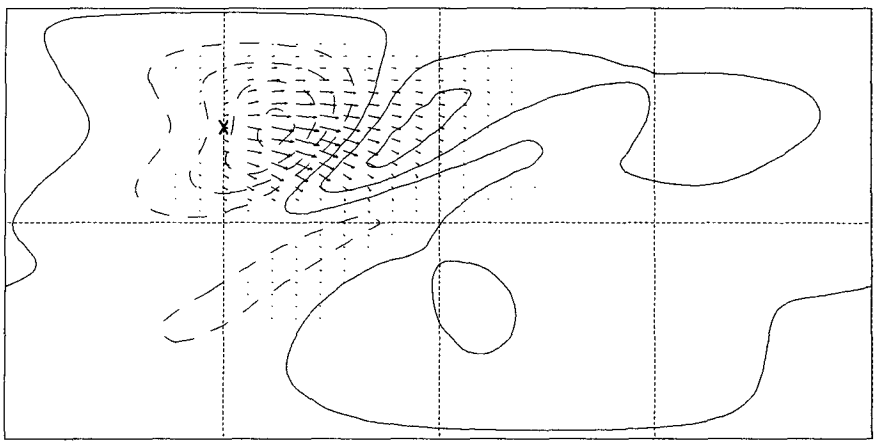

FIG. 10. Plot of wave activity flux vectors **F**, and contours of perturbation streamfunction ψ^*, at day 7 for calculation W05 ($F_0 = 0.05$ and basic state $\mathscr{W}_1$). The contour interval of ψ^* is 2.5×10^6 m^2 s^{-1}.

water pseudospectral calculations show the same wave breaking, formation of a surf zone, and inhibited interhemispheric propagation as in the CS calculations. The results presented are therefore not sensitive to divergence or (small) dissipative effects.

As noted earlier, however, one important aspect of the tropical upper troposphere that is absent from these calculations is the Hadley circulation. Farrell and Watterson (1985) and Watterson and Schneider (1987) have shown that the meridional flow in this circulation can change the equatorward propagation. The study of Held and Phillips (1990) illustrates the displacement of the surf zone off the equator so that, in regions of strong divergent flow (and likely strong equatorial east-

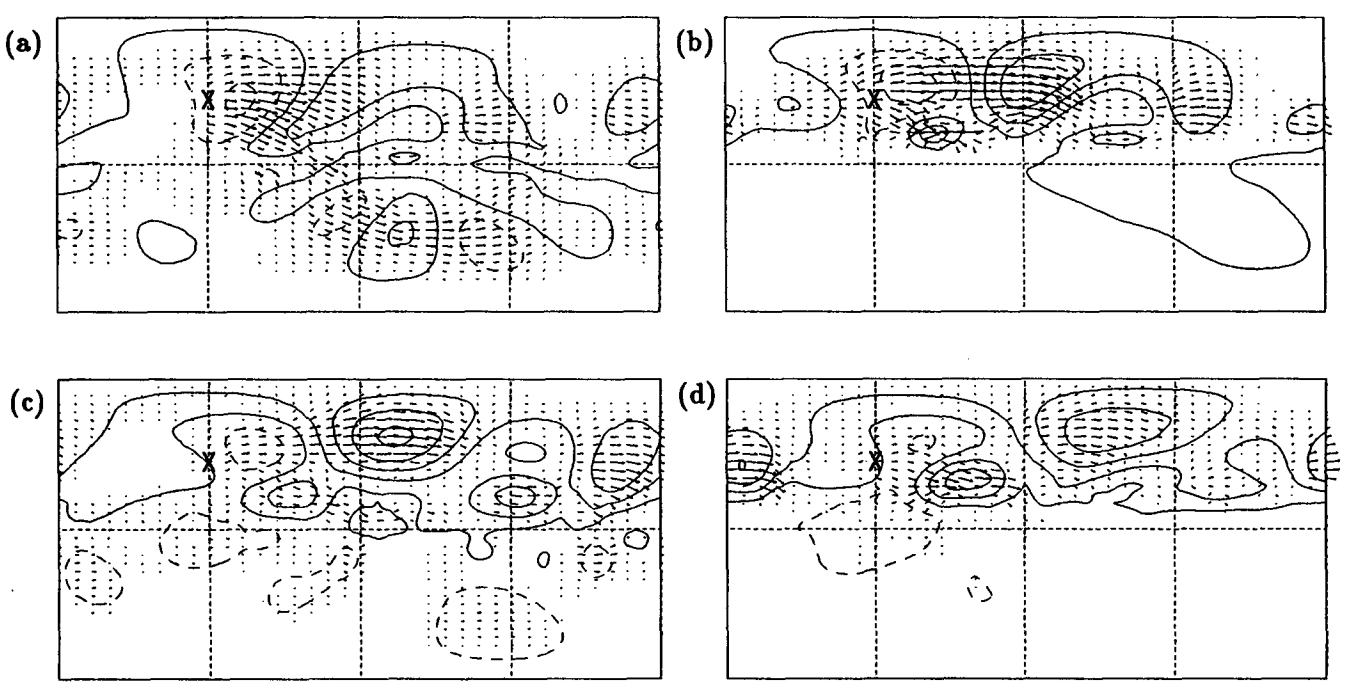

FIG. 11. Plot of wave activity flux vectors **F**, and contours of perturbation streamfunction ψ^*, at day 35 for calculations (a) W05, (b) E05, (c) W20, and (d) E20. The scale of the flux vectors and contour interval in (a) and (b) is the same as in Fig. 10, whereas the vectors in (c) and (d) are smaller by the square of the ratio of the forcing amplitudes (i.e., $(0.20/0.05)^2 = 16$) and the contour interval of ψ^* is 10^7 m^2 s^{-1}.

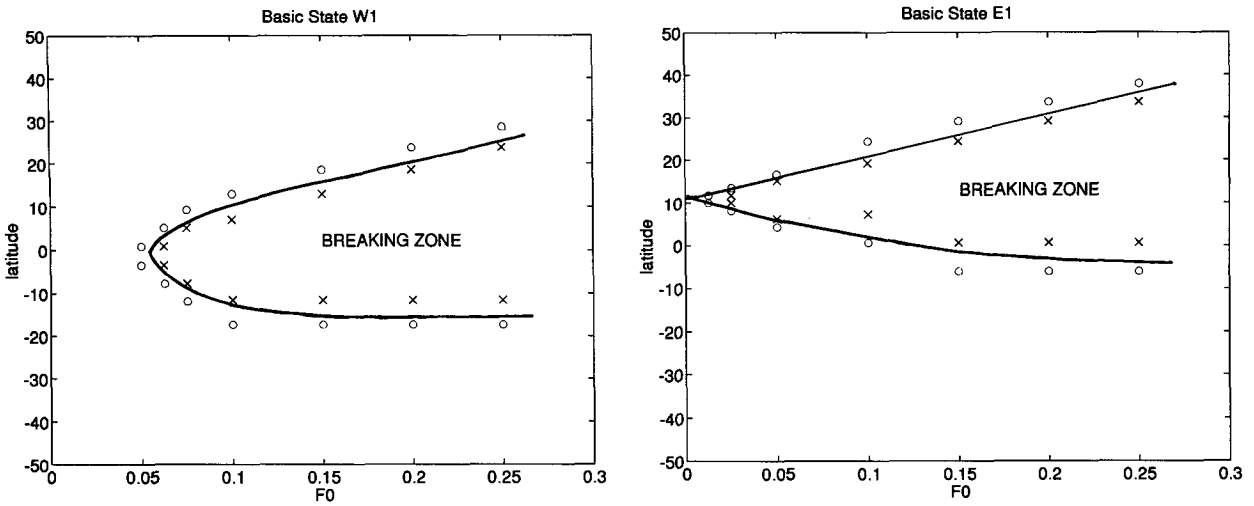

FIG. 12. Variation of surf zone width with forcing amplitude F_0 for (a) basic state $\mathcal{W}_1$, and (b) basic state $\mathcal{E}_1$. A circle corresponds to a contour that remains single valued, and a cross to a contour that becomes double valued. The region between the curves (which have been drawn by hand) corresponds to the region of breaking (surf zone).

erlies), we should expect it to be displaced northward from those shown here. Therefore, the present results may not be directly applicable to the tropical atmosphere as a whole. However, in those parts of the tropics where the Hadley circulation is weak—including the tropical east Pacific region where the upper tropospheric equatorial winds are frequently westerly—the northward displacement should be small. We expect, therefore, that our conclusions regarding cross-equatorial wave propagation through tropical westerlies should not be undermined by this shortcoming of the model.

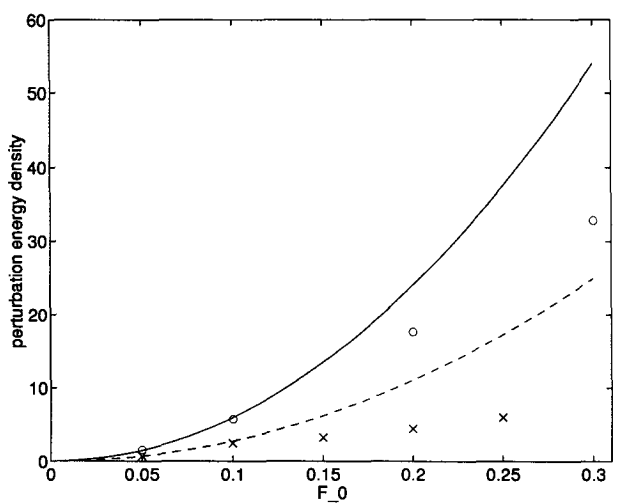

FIG. 13. Variation of Southern Hemisphere perturbation energy ($m^2 s^{-2}$), at day 35, with F_0 for basic states $\mathcal{W}_1$, and $\mathcal{W}_2$. A cross corresponds to a calculation with basic state $\mathcal{W}_1$, and a circle to calculations with basic state $\mathcal{W}_2$. The curves correspond to the energy density predicted by linear theory using the values from calculations with $F_0 = 0.025$ ($\mathcal{W}_1$: dashed curve; $\mathcal{W}_2$: solid curve).

Acknowledgments. We thank the anonymous reviewers for their helpful comments. This work was supported by the National Science Foundation through Grant ATM-9245804. Computations were performed on the Cray Y-MP at the Pittsburgh Supercomputing Center through Grant ATM920001P. The original application of CS to simulations of a topographically forced barotropic atmospheric was developed while DWW was at the Dept. of Applied Mathematics and Theoretical Physics, Cambridge, U.K., with support through the Association of Commonwealth Universities, the U.S. office of Naval Research, and the U.K. Universities' Global Atmospheric Modeling Project.

REFERENCES

Branstator, G. 1983: Horizontal energy propagation in a barotropic atmosphere with meridional and zonal structure. *J. Atmos. Sci.*, **40,** 1689–1708.

——, 1985: Analysis of general circulation sea surface temperature anomaly simulation using a linear model. Part II Eigenanalysis. *J. Atmos. Sci.*, **42,** 2242–2254.

Dritschel, D. G., 1988a: Nonlinear stability bounds for inviscid, two-dimensional, parallel or circular flows with monotonic vorticity, and analogous three-dimensional quasi-geostrophic flows. *J. Fluid Mech.*, **191,** 575–581.

——, 1988b: Contour surgery: A topological reconnection scheme for extended integrations using contour dynamics. *J. Comput. Phys.*, **77,** 240–266.

——, 1989: Contour dynamics and contour surgery: Numerical algorithms for extended, high-resolution modeling of vortex dynamics in two-dimensional, inviscid, incompressible flows. *Comput. Phys. Rep.*, **10,** 77–146.

Farrell, B., and I. Watterson, 1985: Rossby waves in opposing currents. *J. Atmos. Sci.*, **42,** 1746–1755.

Frederiksen, J. S., and P. J. Webster, 1988: Alternative theories of atmospheric teleconnections and low-frequency fluctuations. *Rev. Geophys.*, **26,** 459–494.

Grose, W. L., and B. J. Hoskins, 1979: On the influence of orography on large-scale atmospheric flow. *J. Atmos. Sci.*, **36,** 223–234.

Haynes, P. H., 1987: On the instability of a Rossby-wave critical layer. *J. Fluid Mech.*, **175,** 463–478.

Held, I., 1983: Stationary and quasi-stationary eddies in the extratropical troposphere: Theory. *Large-Scale Dynamical Processes in the Atmosphere,* B. J. Hoskins and R. P. Pearce, Eds., Academic Press, 127–168.

——, and I. S. Kang, 1987: Barotropic models of the extratropical response to El Niño. *J. Atmos. Sci.*, **44,** 3576–3586.

——, and P. J. Phillips, 1990: A barotropic model of the interaction between the Hadley cell and a Rossby wave. *J. Atmos. Sci.*, **47,** 856–869.

Hoskins, B. J., and D. J. Karoly, 1981: The steady linear response of a spherical atmosphere to thermal and orthographic forcing. *J. Atmos. Sci.*, **38,** 1179–1196.

——, A. J. Simmons, and D. G. Andrews, 1977: Energy dispersion in a barotropic atmosphere. *Quart. J. Roy. Meteor. Soc.*, **103,** 553–567.

Lau, K. M., and H. Lim, 1984: On the dynamics of equatorial forcing of climate teleconnections. *J. Atmos. Sci.*, **41,** 161–176.

Lau, N. C., 1984: Circulation statistics based on FGGE level IIIb analyses performed by GFDL. NOAA Data Report ERC GFD-5, 427 pp.

——, G. H. White, and R. C. Jenne, 1981: Circulation statistics for the extratropical Northern Hemisphere based on NMC analyses. NCAR Tech. Note NCAR/TN-171+STR, 128 pp.

Legras, B., and D. G. Dritschel, 1993: A comparison of the contour surgery and pseudo-spectral methods. *J. Comput. Phys.*, **104,** 287–302.

Longuet-Higgins, M. S., 1964: Planetary waves on a rotating sphere, I. *Proc. Roy. Soc. London,* **A279,** 446–473.

McIntyre, M. E., and T. N. Palmer, 1983: Breaking planetary waves in the stratosphere. *Nature,* **305,** 593–600.

——, and ——, 1984: The 'surf zone' in the stratosphere. *J. Atmos. Terr. Phys.*, **46,** 825–849.

——, and T. G. Shepherd, 1987: An exact local conservation theorem for finite-amplitude disturbances to non-parallel shear flows, with remarks on Hamiltonian structure and Arnold's stability theorems. *J. Fluid Mech.*, **181,** 527–565.

Plumb, R. A., 1985: On the three-dimensional propagation of stationary waves. *J. Atmos. Sci.*, **42,** 217–229.

Polvani, L. M., and R. A. Plumb, 1992: Rossby wave breaking, filamentation and secondary vortex formation: The dynamics of a perturbed vortex. *J. Atmos. Sci.*, **49,** 462–476.

——, and D. G. Dritschel, 1993: Wave and vortex dynamics on the surface of a sphere. *J. Fluid Mech.*, **255,** 35–64.

——, G. R. Flierl, and N. J. Zabusky, 1989: Filamentation of unstable vortex structures via separatrix crossing: A quantitative estimate of onset time. *Phys. Fluids A,* **1,** 181–183.

Sardeshmukh, P. D., and B. J. Hoskins, 1988: The generation of global rotational flow by steady linearized tropical divergence. *J. Atmos. Sci.*, **45,** 1228–1251.

Simmons, A. J., 1983: The forcing of stationary wave motion by tropical diabatic heating. *Quart. J. Roy. Meteor. Soc.*, **108,** 503–534.

——, J. M. Wallace, and G. W. Branstator, 1983: Barotropic wave propagation and instability, and atmospheric teleconnection patterns. *J. Atmos. Sci.*, **40,** 1363–1392.

Tomas, R. A., and P. J. Webster, 1994: Horizontal and vertical structure of cross-equatorial wave propagation. *J. Atmos. Sci.*, **51,** 1417–1430.

Watterson, I. G., and E. K. Schneider, 1987: The effect of the Hadley circulation on the meridional propagation of stationary waves. *Quart. J. Roy. Meteor. Soc.*, **113,** 779–813.

Waugh, D. W., 1993: Contour surgery simulations of a forced polar vortex. *J. Atmos. Sci.*, **50,** 714–730.

Webster, P. J., 1981: Mechanisms determining the atmospheric response to sea surface temperature anomalies. *J. Atmos. Sci.*, **38,** 544–571.

——, and J. R. Holton, 1982: Cross-equatorial response to middle-latitude forcing in a zonally varying basic state. *J. Atmos. Sci.*, **39,** 722–733.

Zabusky, N. J., M. H. Hughes, and K. V. Roberts, 1979: Contour dynamics of the Euler equations in two-dimensions. *J. Comput. Phys.*, **30,** 96–106.